



Science Arts & Métiers (SAM)

is an open access repository that collects the work of Arts et Métiers Institute of Technology researchers and makes it freely available over the web where possible.

This is an author-deposited version published in: <https://sam.ensam.eu>
Handle ID: <http://hdl.handle.net/10985/20616>

To cite this version :

Paul KERDRAON, Boris HOREL, Patrick BOT, Adrien LETOURNEUR, David DAVID LE TOUZÉ - High Froude Number Experimental Investigation of the 2 DOF Behavior of a Multihull Float in Head Waves - Journal of Sailing Technology - Vol. 6, n°01, p.1-20 - 2021

Any correspondence concerning this service should be sent to the repository

Administrator : scienceouverte@ensam.eu



High Froude Number Experimental Investigation of the 2 DOF Behavior of a Multihull Float in Head Waves

Paul Kerdraon

VPLP Design, France and Ecole Centrale Nantes, France, kerdraon@vannes.vplp.fr

Boris Horel

Ecole Centrale Nantes, LHEEA Laboratory (ECN and CNRS), France

Patrick Bot

Naval Academy Research Institute, France

Adrien Letourneur

VPLP Design, France

David Le Touzé

Ecole Centrale Nantes, LHEEA Laboratory (ECN and CNRS), France

Manuscript received 22 September 2020; revision received January 4, 2021; accepted February 3, 2021.

Abstract. Dynamic Velocity Prediction Programs are taking an increasingly prominent role in high performance yacht design, as they allow to deal with seakeeping abilities and stability issues. Their validation is however often neglected for lack of time and data.

This paper presents an experimental campaign carried out in the towing tank of the Ecole Centrale de Nantes, France, to validate the hull modeling in use in a previously presented Dynamic Velocity Prediction Program. Even though with foils, hulls are less frequently immersed, a reliable hull modeling is necessary to properly simulate the critical transient phases such as touchdowns and takeoffs.

The model is a multihull float with a waterline length of 2.5 m. Measurements were made in head waves in both captive and semi-captive conditions (free to heave and pitch), with the model towed at constant yaw and speed. To get as close as possible to real sailing conditions, experiments were made at both zero and non-zero leeway angles, sweeping a wide range of speed values, with Froude numbers up to 1.2. Both linear and nonlinear wave conditions were studied in order to test the limits of the modeling approach, with wave steepness reaching up to 7% in captive conditions and 3.5% in semi-captive ones.

The paper presents the design and methodology of the experiments, as well as comparisons of measured loads and motions with simulations. Loads are shown to be consistent, with a good representation of the sustained non-linearities. Pitch and heave motions depict an encouraging correlation which confirms that the modeling approach is valid.

Keywords: DVPP; towing tests; seakeeping; high Froude number; validation.

NOMENCLATURE

| | |
|----------|---------------------------------------|
| A | Wave amplitude [m] |
| f | Frequency [Hz] |
| F_n | Froude number [-] |
| h | Tank depth [m] |
| I_{yy} | Inertia in pitch [kg m ²] |
| LCG | Longitudinal center of gravity [m] |

| | |
|------------|--|
| L_{PP} | Length between perpendiculars [m] |
| m | Oscillating mass [kg] |
| S | Wave steepness ($2A/\lambda$) [-] |
| T | Wave period [s] |
| V | Carriage speed [m s^{-1}] |
| VCG | Vertical Center of Gravity [m] |
| β | Leeway angle [$^{\circ}$] |
| δ | Distance between center of gravity and rotation axis [m] |
| λ | Wavelength [m] |
| ω | Wave frequency [rad s^{-1}] |
| ω_e | Frequency of encounter [rad s^{-1}] |
| DOF | Degree of Freedom |
| DVPP | Dynamic Velocity Prediction Program |
| IMU | Inertial Measurement Unit |
| ITTC | International Towing Tank Conference |

1. INTRODUCTION

With the development of foiling, accurate trade-offs between stability and performance are critical in offshore racing yacht design. Dynamic simulation which allows assessing these criteria has thus taken a central role in the design process. Angelou and Spyrou (2017) have for instance simulated the behavior in waves of a cruiser and especially the occurrence of surf-riding in downwind conditions. Simulation of foiling yachts (e.g., Hansen *et al.* 2019; Horel and Durand 2019) has drawn a particular interest from the high-performance community as it allows to test extensively different design options and yacht configurations.

The numerical tools on which these simulations rely, called DVPPs (Dynamic Velocity Prediction Programs), often use modeling approaches beyond their original scope of validity, such as linear seakeeping theory at high Froude numbers or in steep waves. The validation tests carried out are often very simple test cases (low Froude number, low steepness waves), rather far from offshore sailing conditions. Similarly, available data for validation mainly focus on power boats and are often limited to rather low Froude numbers (ITTC 2017c, 2017d).

Validation of a DVPP as a whole is complex as it involves many parameters and couplings, especially when high performance yachts fitted with state-of-the-art appendages are concerned. In the process of validation, two approaches are possible: full-scale tests and model experiments.

Full scale tests are of great interest as they allow to directly compare predictions to reality. However, validating a simulation code implies that the behavior in all situations of interest as well as the characteristics of all modeled phenomena are sufficiently repeatable. Conducting the standard ship maneuvers (turning circle, zig-zag tests, etc.) both numerically and in full scale is thus a good starting point for assessing the quality of a maneuvering model. However, this is poorly suited for the specialties of sailing yachts.

Several attempts to validate sailing yacht simulation codes with full scale tests have been reported (see for instance Masuyama *et al.* 1993; Masuyama and Fukasawa 2011; Day *et al.* 2002; Binns *et al.* 2008; Clark 2014). They allowed to point out the shortcomings and strong points of the models. To gain confidence, in the numerical tool, exhaustive tests must be successively and rigorously carried out. Binns *et al.* (2008) have thus proposed a 6 tests procedure, each of them designed to assess specific aspects of the simulation models (hydrodynamic added mass, damping, etc.).

Full-scale tests face nonetheless two major difficulties: the evaluation of the environmental conditions and the quantity of available data. Day *et al.* (2019) pointed out the challenges of full-scale testing in open water. As reported in the International Towing Tank Conference (ITTC) recommendations (ITTC 2017c), the complexity of documenting the environmental conditions (wind, waves, currents) properly and exhaustively during the whole test sessions degrades the data quality. The quantification of the environmental parameters and their fluctuations within the whole area covered by the yacht during measurement session is difficult.

Besides, while measuring speed, position or attitudes is nowadays rather convenient with on board equipment or small measuring units, the assessment of some data remains complex and expensive. For instance, as the complexity of state-of-the-art high-performance appendages and their available tunings (flap, rake, cant, extension) have much increased in the recent years, the knowledge of the deflections and loads they sustain is now critical in the understanding of their behavior.

The characterization and enforcement of the environmental conditions is much easier in model tests. Nevertheless, two other issues need to be tackled. First the incompatibility between Froude and Reynolds similarities is questionable especially for the scaling of the appendage loads. Second the propelling of the model is a complex matter if one is willing to account for the heeling and pitching moments as well as the unsteady aerodynamic effects. A first approach introduced by Allan *et al.* (1957), referred to as *free sailing* tests, consists in towing the model at the aerodynamic center of effort with constant tension. In this way, the model sails with a realistic attitude. However, in addition to the equilibrium settlement issues reported by Murdey *et al.* (1987), this method does not allow to vary dynamically the position of the center of effort or the aerodynamic force direction and magnitude. A very promising approach developed recently at the Wolfson Unit and presented by Gauvain (2019) allows to avoid these issues by using an air screw device mounted on a mast to generate a variable propulsion force.

In parallel, semi-captive tests remain very popular for seakeeping experiments. The model is linked to the towing carriage with at least two free degrees of freedom, heave and pitch. This approach allows to compare the predicted motion in waves with full control over the conditions. When trying to validate a system-based DVPP, where loads are computed by dividing the yacht in several components (appendages, hull, etc.) and summing up their contributions, a particular interest of getting back to simpler methods as semi-captive tests is that they allow to isolate specific model blocks and validate them independently of each other.

This is the approach chosen herein, with the aim of validating the hull modeling of a DVPP presented in Kerdraon *et al.* (2019, 2020). This paper first details the design and setup of the experimental campaign, before presenting some of the resulting data. A comparison is done between the experiments and their numerical modeling in the DVPP, and concluding remarks are finally given.

2. TEST DESIGN

2.1. Organization

The experimental campaign took place from April to June 2019. The present paper is interested in the first stage of the campaign, which was dedicated to the study of motions and loads in waves. Tests were carried out both in restrained conditions (wave loads study) and with two degrees of freedom (heave and pitch responses study).

2.2. Tank facility and setup

Experiments were carried out in the towing tank facility of the LHEEA laboratory in Nantes, France. The tank is 140 m-long, 5 m-wide, and has a 3 m constant depth. A hydraulic flap-type wave-maker equips one end of the tank, while on the other end a wave absorber limits wave reflection. The towing carriage has a theoretical maximum speed of 8 m/s.

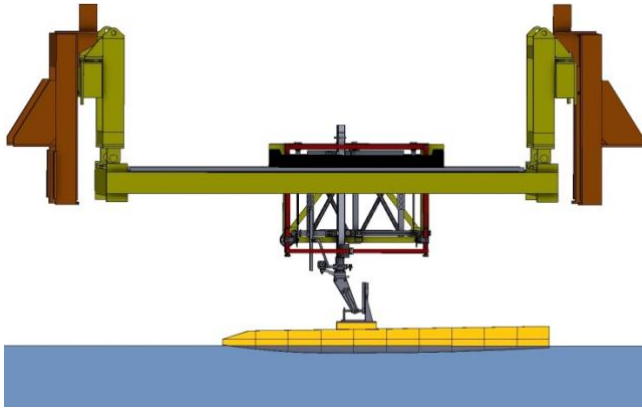


Figure 1. Example of a figure.

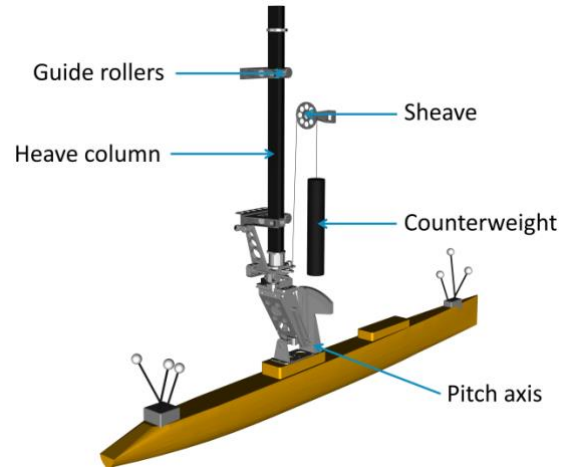


Figure 2. The heave and pitch system.

The experimental setup is presented in Figures 1 and 2. The model is held by an orienting device that allows the adjustment of yaw, pitch and heel. Pitch and heel can be independently freed or restrained with a lock-pin system, while yaw is adjustable through a worm screw. Model and orienting device are linked to the load cell by a column allowed to slide vertically guided by two sets of three rollers. A counterweight system allows to compensate for the weight of the column and pitch system, and set the model displacement at the target value. The column can be prevented from moving by a clamping system.

2.3. Model

2.3.1 Geometric properties

Offshore racing multihulls floats are characterized by very high slenderness and rather shallow draft. A 2.5 m long model with such properties was used. In comparison with a 100 ft-Ultim trimaran, this represents a scale factor of 12.8. Its main characteristics are given in Table 1 and Figure 3.

Table 1. Model geometric properties.

| | | |
|-------------------------------|----------|---------|
| Length between perpendiculars | L_{PP} | 2.500 m |
| Waterline length | LWL | 2.490 m |
| Waterline breadth | BWL | 0.115 m |
| Draft | d | 0.057 m |

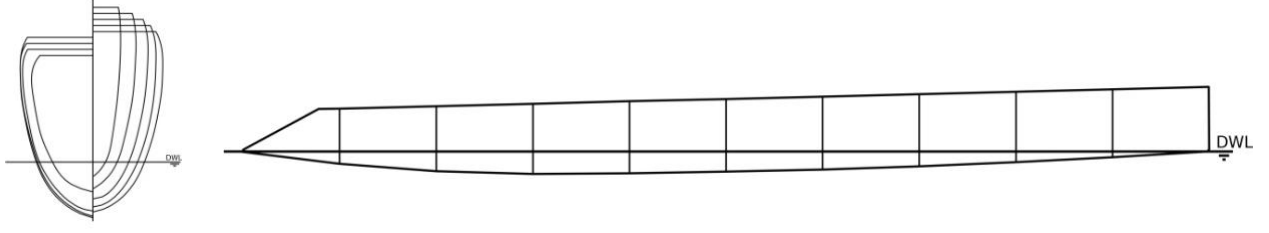


Figure 3. Model body plan.

As explained in the introduction, the aim of the experimental campaign is to validate the hull modeling. Thus, only a single bare hull was used with neither appendages nor superstructure.

To stimulate turbulence and ensure equivalence of the model-scale regime with the full-scale one, the model is fitted with three 10 mm-wide sand stripes spaced by 50 mm and located at $10\%L_{PP}$ (see ITTC guidelines, ITTC 2017b).

2.3.2 Inertial properties

The longitudinal position of the center of gravity (LCG) and the displacement were defined to reach an attitude that is consistent for modern geometries (see Table 2) the transom is slightly immersed, while the bow skims the free surface. As far as the vertical position of the center of gravity (VCG) is concerned, it was defined scaling the full-scale value of a complete trimaran.

Table 2. Model inertial properties.

| | | |
|------------------------|----------|------------------------|
| Target displacement | ∇ | 6.0 kg |
| LCG (measure) | LCG | 1.018 m |
| VCG (measure) | VCG | 0.192 m |
| Inertia in pitch at CG | I_{yy} | 16.4 kg m ² |

A polyurethane foam platform was fitted to install the orienting device, with the pitching axis right above the target LCG value. The model was suspended to a gantry by the orienting device. Inclination tests were performed with calibration masses and an inclinometer to measure the position of the center of gravity. Masses were fitted to the model to correct the measured value iteratively until satisfactory measurements were obtained: the effective LCG is 2 mm behind the target value, corresponding to a pitch angle variation of less than 0.01° .

The chosen LCG being rather backwards (40% of L_{PP}), it was necessary to add an important amount of weight at the stern. Consequently, the pitch inertia is proportionally much higher than it should. It was measured performing oscillations tests on the same setup, and measuring the period T , which is linked to the inertia in pitch I_{yy} by the relation:

$$T = 2\pi \sqrt{\frac{I_{yy}}{m g \delta}}$$

where m is the total mass oscillating in pitch (including the moving part of the orienting device) and δ the distance between center of gravity and rotation axis. Usually, pitch radius of inertia is of the order of $0.25L_{PP}$, whereas, accounting for all the elements moving in pitch, the equivalent radius for the setup is $0.52L_{PP}$. Consequences are discussed in section 3.4.

2.4. Instrumentation

2.4.1 Load cell

The in-house load cell provides measurements for the 6 force components using strain gauges. All gauges are held by thin decoupling rods to minimize cross-axis sensitivity and interference between loads. One sensor is oriented in the tank direction, two (front and rear parts) in the transverse direction and three (front, middle and rear parts) in the vertical direction, with the middle one shifted transversely with respect to the others. Their combination allows to derive the moments. When heave and pitch are freed, the corresponding loads only represent frictions in the setup.

The load cell was calibrated before and after the experimental campaign to check for possible alteration of the sensors. No significant variation of the conversion coefficients was observed (less than 0.2%). A calibration chassis, directly mounted on the load cell frame and equipped with sheaves, allows to load each of the gauges at known positions with low misalignment errors. A linear least-square regression is used to derive the calibration matrix.

2.4.2 Other measurements

The measurements of the model attitudes is redundant so that if one sensor fails other measurements are available. Rotating potentiometers directly fitted on the orienting device are used to measure yaw and pitch angles, while a laser on the sliding column measures the heave motion. An inertial measurement unit (IMU, SBG Ellipse 2E) records model attitudes and accelerations.

The position of the carriage is measured by incremental encoders on each side of the carriage. Its derivative allows to retrieve the carriage speed.

Two ultrasonic wave probes located at different longitudinal positions (bow and center of gravity) are used to measure the free surface elevation and retrieve the excitation phase.

Finally, a trajectory motion capture system (Qualisys) tracks the positions of two reference elements respectively located at the bow and stern of the model (white spheres in Figure 4).

2.4.3 Acquisition

Potentiometers, carriage speed and positions, wave probes, heave laser sensor and load cells are plugged to a first acquisition module (HBM MX1615B) while the inertial measurement unit (SBG Ellipse 2E) is plugged into a second one (HBM M840B). Both modules are linked and thus synchronized by the acquisition program. The sample rate was set to 100 Hz.

The motion capture system (Qualisys) was running on a second computer, with a separate acquisition software. An experimental issue with the triggering system prevented a correct synchronization between the two acquisitions so that a phase shift exists between the tracking measurements and the other data. Inertial unit and potentiometers allowing the determination of the motion phase, this issue was however not critical.

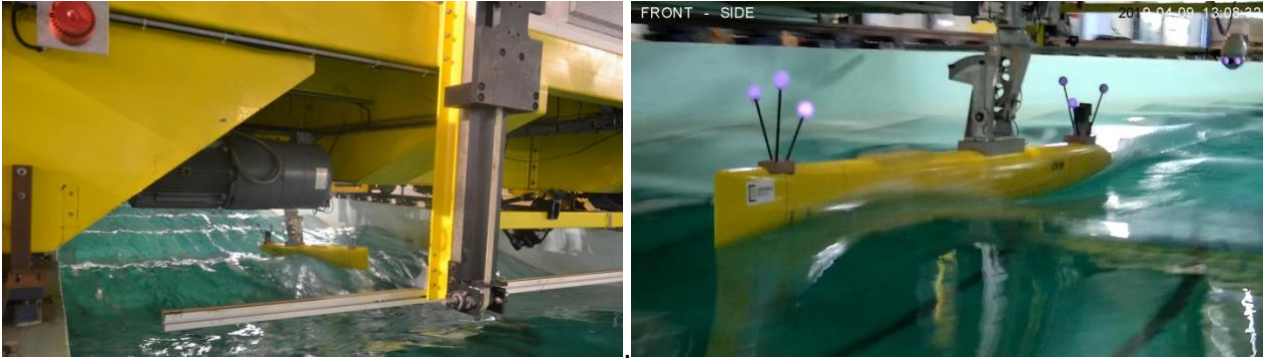


Figure 4. Semi-captive tests in head waves with (right) and without (left) forward speed.

2.5. Test parameters

As the heel angle of multihulls, especially with foils, tends to be rather small in absolute value, all experiments were carried out upright to focus on parameters that were believed to be more relevant.

The presented setup was used during three measurement steps, with the model towed at constant speed and yaw:

- Straight line towing on flat water, with 2DOF: to measure loads and reference attitudes,
- Captive tests in waves: to measure the wave loads and compare with the models,
- Semi-captive tests in waves (Figure 4): to measure the heave and pitch response and compare with simulations.

Four speed values were swept as well as 2 leeway angles. Details are given in Table 3.

Table 3. Speed and leeway conditions at model scale.

| Speed (m/s) | Froude number (-) | Leeway angle (°) |
|-------------|-------------------|------------------|
| 0 | 0.00 | 0.0 |
| 1.8 | 0.36 | 0.0 |
| 4.0 | 0.81 | 2.0 |
| 6.0 | 1.21 | 2.0 |

It was found more relevant to study head wave conditions, in which the pitch and heave responses are of greater importance. To simplify the problem, only monochromatic waves were studied. In the objective of studying the model response at diverse Froude values as well as for both small and steep waves, it was chosen not to sweep a wide number of wave periods but to concentrate on two values. To define those values, the response amplitude operators at zero speed were computed using a seakeeping potential code. They are plotted in Figure 5. The heave response does not exhibit any resonance, but the pitch one has a peak towards which a first value of wave frequency was defined. The second value was chosen to lie at higher frequencies, but still on the peak. Besides, those two values lead to wavelength of the order of respectively $2L_{PP}$ and L_{PP} , which are conditions of known interest. Two amplitudes were studied for both wave periods (see Table 4), the resulting steepness values $S = 2A/\lambda$ were respectively 1.5% / 3.5% and 1.5% / 7.0%.

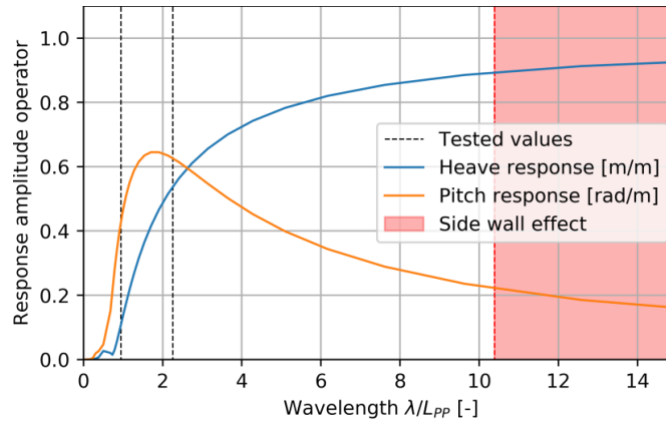


Figure 5. Heave and pitch response amplitude operators at $F_n=0$.

For the forward speed cases, two schemes were tested. In the first one, the wave properties were kept constant, so that the encounter frequency, ω_e , increased. In the second one, the encounter frequency was kept constant, as well as the amplitude, so that tested wavelength increased (and wave steepness decreased). Wave tested conditions are summarized in Table 4.

When pitch and heave were freed, some of the harshest wave conditions lead to too large motions that were blocked by the heave and pitch systems stops. No measurement was thus possible in 2DOF for the 7% steepness waves.

Table 4. Wave conditions.

| Fn (-) | Constant ω | | Constant ω_e | |
|--------|------------------------|-------|------------------------|-------|
| | λ / L_{PP} (-) | S (-) | λ / L_{PP} (-) | S (-) |
| 0 | 2.25 | 1.5% | 2.25 | 1.5% |
| | | 3.5% | | 3.5% |
| | 0.94 | 1.5% | 0.94 | 1.5% |
| | | 7.0% | | 7.0% |
| 1.8 | 2.25 | 1.5% | 4.59 | 0.7% |
| | | 3.5% | | 1.7% |
| | 0.94 | 1.5% | 2.40 | 0.6% |
| | | 7.0% | | 2.8% |
| 4 | 2.25 | 1.5% | 7.05 | 0.5% |
| | | 3.5% | | 1.1% |
| | 0.94 | 1.5% | 3.87 | 0.4% |
| | | 7.0% | | 1.7% |
| 6 | 2.25 | 1.5% | 9.16 | 0.4% |
| | | 3.5% | | 0.9% |
| | 0.94 | 1.5% | 5.18 | 0.3% |
| | | 7.0% | | 1.3% |

2.5. Guidelines

To avoid side wall effects when carrying out seakeeping experiments, IITC (2017a) recommends that the upper wavelength in head waves remains below a value given as a function of the model length, the tank width and the Froude number F_n . This is necessary to avoid that the reflected waves catch up with the model. The formula is based on the consideration of a harmonic strength source. The larger the Froude number the larger the available wavelength range. Obviously, at $F_n = 0$, interference happens and only the data before reflected waves come back to the ship are to be accounted for. The lower wavelength bound for the stricter condition $F_n = 0.36$ is $10.4L_{pp}$, all considered waves are below this limit.

DeBord *et al.* (1990) add that the model submerged cross section should be less than 1/100 of the tank cross section to minimize blockage effects. This condition is validated as the model cross section is only 0.0044 m^2 , which represents less than 1/3000 of the $5 \times 3 \text{ m}$ tank cross section.

While the model draft to tank depth ratio is negligible, the critical wave velocity $V_{crit} = \sqrt{gh}$ is rather small ($V_{crit} = 5.4 \text{ m/s}$). DeBord *et al.* (1990) advise not to neglect the tank finite depth if the test speeds are beyond 70% of the critical wave velocity, which is the case for the two highest speed values. This point is discussed in further details in 4.4.

3. RESULTS

3.1. Noise and filtering

Especially at the highest speeds, measurements are perturbed by high frequency components induced by vibrations of diverse origins. It is of interest to identify the causes and characteristics of these vibrations to deal with them adequately.

Frequency analysis on flat water towing tests allows to identify two vibration components. The first one ($V / f \simeq 25\text{-}30 \text{ m}$) corresponds to carriage superstructure vibrations, while the second ($V / f \simeq 0.72 \text{ m}$) corresponds to the rail plates presence. While potentiometers measurements are relatively unaffected by noises (Figure 6a), other instruments such as the inertial unit are much more perturbed, mainly around 8 Hz (Figure 6b).

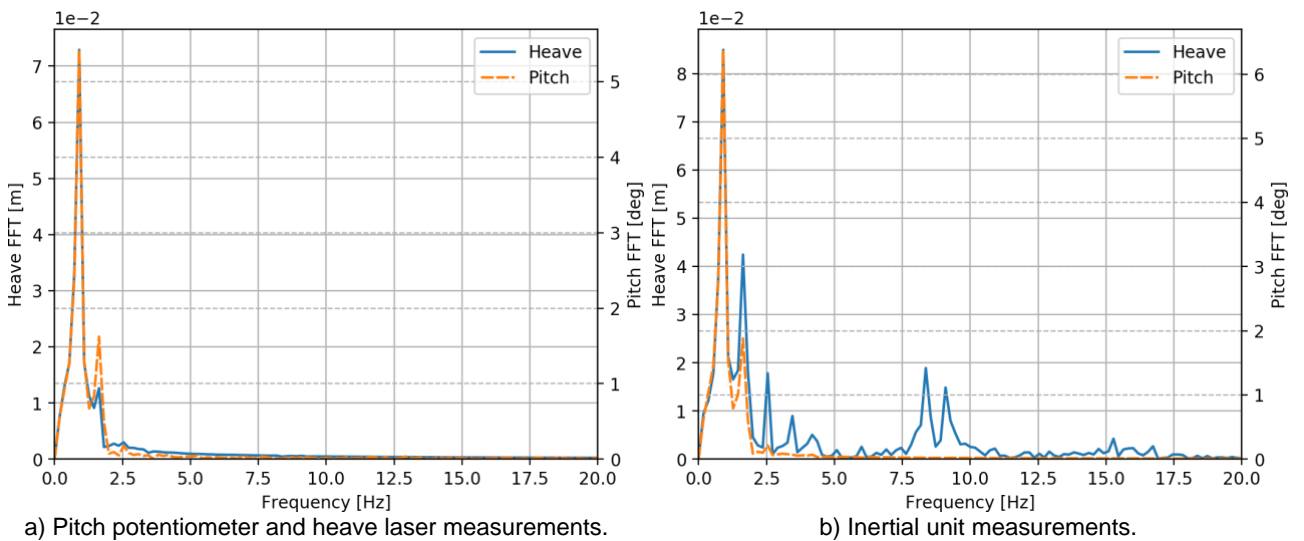


Figure 6. Spectra of the heave and pitch responses at $F_n = 1.21$, $\beta = 0^\circ$, $\lambda = 5.2L_{pp}$ and $S = 0.6\%$.

The first vibration component is too close to the frequency range of interest to be filtered. But the second one, as well as the high frequency noise can be filtered using a low-pass filter. A Butterworth type filter is used and applied twice, once forward and once backward so that the implied phase delay is removed. The effective order of such method is twice the order of the initial filter. The highest encounter frequency of the test matrix is 3.34 Hz, a cut frequency of 4.5 Hz and a filter order of 5 is thus used. At 3.34 Hz the filter gain is then -0.01 dB, while at about 8.0 Hz it falls to -50 dB, which seems a good compromise between not altering the signal of interest and removing the perturbations. Higher order filters could be used to decrease even further the high frequency components, but it increases the probability of numerical instabilities. One should however take precautions when filtering the signals as it may smooth interesting harsh non-linearities in the response. Hence, raw signals are systematically checked and compared to filtered signals.

3.2. Repeatability

A number of runs were performed several times to check the repeatability of the experiments. All repeated tests were carried out within one week. Initial conditions are similar in terms of speed evolution and history of encountered waves (timing of the wave front arrival) as the carriage and wave-maker are synchronized. Carriage stop was either manual or automatic, the deceleration phase may thus vary between tests.

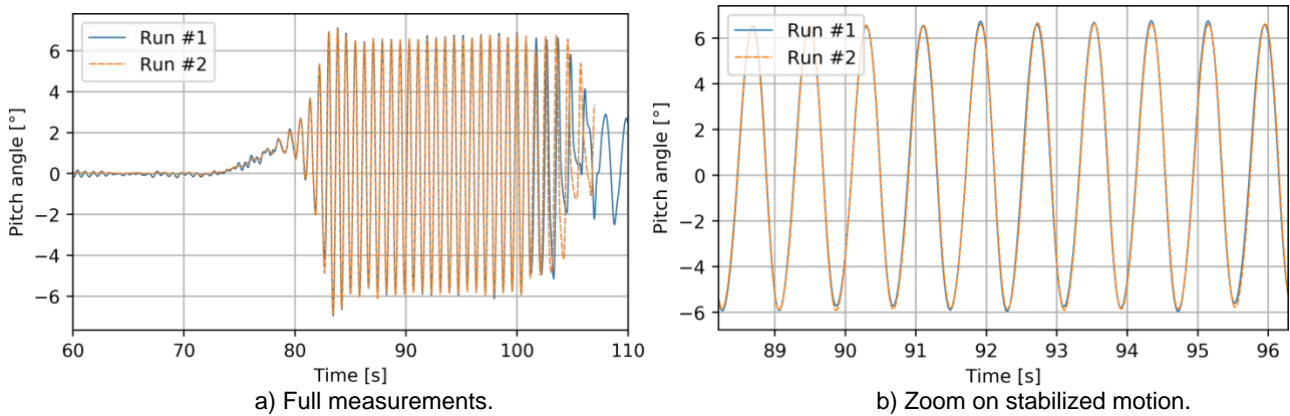


Figure 7. Repeated tests example, pitch angle from inertial unit, at $F_n = 0.81$, $\beta = 0^\circ$, $\lambda = 2.25L_{pp}$ and $S = 1.5\%$.

Figure 7 shows the pitch signal superposition of two repeated tests for the conditions $F_n = 0.81$, $\lambda = 2.25L_{pp}$ and $S = 1.5\%$. Correlation between both tests is good. When fitting the stabilized oscillations by a sine function $a + b \sin[\omega_e(t + c)]$, the differences between the fitted coefficients are small as shown on Table 5.

Table 5. Comparison of the fitted coefficients for function $a + b \sin[\omega_e(t + c)]$.

| Coefficients | Run #1 | Run #2 | Difference |
|--------------|--------|--------|------------|
| a (°) | 0.329 | 0.292 | 0.037 |
| b (°) | 6.286 | 6.293 | 0.007 |
| c (s) | 0.482 | 0.428 | 0.054 |

3.3. Uncertainties

Seven categories of uncertainty causes have been identified in the experiment:

- Model (dimensions, wetted surface, center of gravity position, displacement, inertia)
- Heave and pitch system (friction, misalignment)
- Carriage speed
- Acquisition system
- Environment (water temperature, waves characteristics)
- Motion sensors (potentiometers, laser, tracking system)
- Load sensors (load cell)

Uncertainties on model properties are summarized in Table 6. Whenever repeated measurements were not carried out (type A uncertainties: standard deviation), type B uncertainties are applied. Combined uncertainties are evaluated through the law of propagation of uncertainty (ITTC, 2014), they are noted as “-” in Table 6.

Table 6. Model uncertainties.

| Variable | Std. uncertainty | Type |
|-------------------|---------------------------------------|------|
| Linear dimensions | $2.9 \cdot 10^{-4} \text{ m}$ | B |
| Mass | $2.9 \cdot 10^{-4} \text{ kg}$ | B |
| Water temperature | 0.1° | B |
| Water density | $2.1 \cdot 10^{-2} \text{ kg m}^{-3}$ | B |
| Displ. volume | $3.1 \cdot 10^{-7} \text{ m}^3$ | - |
| LCG | $1.4 \cdot 10^{-5} \text{ m}$ | A |
| VCG | $1.0 \cdot 10^{-4} \text{ m}$ | A |
| Inertia | $3.2 \cdot 10^{-2} \text{ kg.m}^2$ | - |

Table 7. Motion sensors uncertainties.

| Sensor | Std. uncertainty |
|---------------------|-------------------------------|
| Pitch potentiometer | $3.7 \cdot 10^{-2}^\circ$ |
| Yaw potentiometer | $3.7 \cdot 10^{-2}^\circ$ |
| Heave laser | $1.0 \cdot 10^{-4} \text{ m}$ |
| IMU angles | 0.1° |

Uncertainty due to friction in the setup was not quantified, but the order of magnitude was evaluated (see 4.4). The load cell was mounted on the carriage using a laser pointer, the accuracy of the assembly is evaluated at about $\pm 1 \text{ mm}$. The carriage speed is measured by two incremental encoders and the standard uncertainty is established at 0.01 m/s . The accuracy class of the acquisition modules is 0.05% according to the supplier.

As far as the uncertainties in the environment are concerned, the measurement of temperature was repeated during the experimental campaign and no significant variation was observed. The accuracy on the wave properties measurements is reported to be better than $3 \cdot 10^{-3} \text{ m}$ by the manufacturer.

The uncertainty with the motion sensors is known from the suppliers' data or from the calibration procedures. They are reported in Table 7. The positions of the IMU and of the orienting device which carries the potentiometers were pinpointed with the CNC milling machine used to process the deck of the model.

Finally, the uncertainties linked to the load cell other than its mounting on the carriage are the calibration uncertainties. The load cell is equipped with a sheave system that minimize misalignment errors during calibration. The uncertainties in the positions of the sheaves are

estimated at 0.5 mm. Calibration mass tolerance is 0.01%. The uncertainty in the curve fitting that allows to express the calibration matrix is given by the standard error of estimation (SEE) (ITTC, 2017a), which based on the 66 calibration points is less than $2.9 \cdot 10^{-2}$ N for forces and $1.4 \cdot 10^{-2}$ Nm for moments.

In resistance tests or linear seakeeping measurements, the output parameters are a finite set of values (drag coefficient, amplitude, phase angle, etc.), this is not the case for nonlinear seakeeping experiments. A way to use statistics methods on the presented experiments is to superpose consecutive periods of the output signals and measure the variations with respect to the mean signal over a period. Figure 8 illustrates the process by plotting $\text{signal}(t) = f(\text{mod}(t, T))$. The computation of the standard deviation of the superposed signal over a period gives an estimation of the data scatter. For the plotted signal, the maximum standard deviation is $1.0 \cdot 10^{-4}$ m.

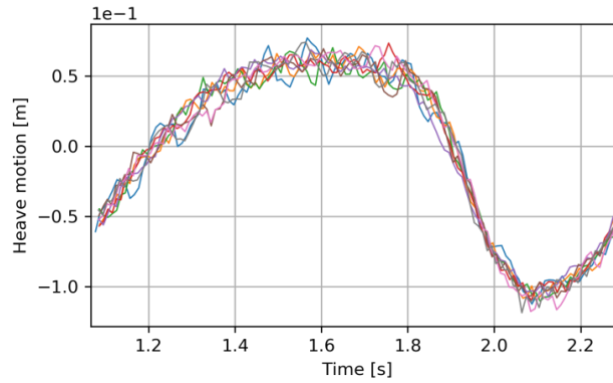


Figure 8. Superposition of the periodic samples on case $F_n = 0.81$, $\beta = 0^\circ$, $\lambda = 3.9L_{PP}$ and $S = 0.9\%$.

3.4. Measurements discussion

As expected, results show linear behavior for the small speeds and wave steepness, while non-linearities alter the amplitudes and shapes of the signals when conditions are tougher. Interesting features especially in pitch are visible in Figure 9, they are believed to be caused by the rather aft position of the model center of gravity.

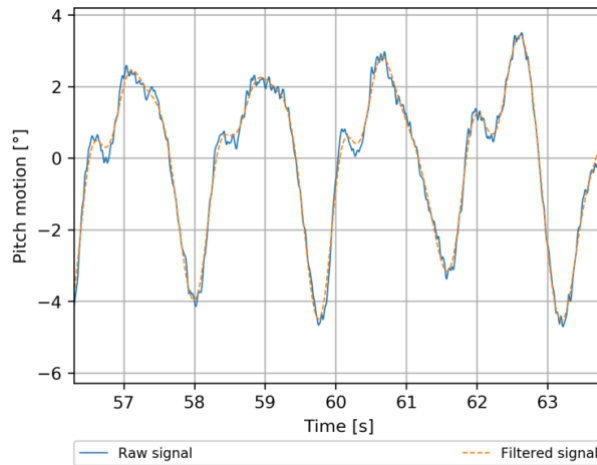


Figure 9. Non-linear pitch angle behavior in regular waves $F_n = 0.81$, $\beta = 0^\circ$, $\lambda = 7.1L_{PP}$ and $S = 1.1\%$.

In some test conditions, it was not possible to reach a stabilized model behavior and the measurements exhibit oscillations of variable amplitudes. This is further complicated at high speeds, where the effective distance remaining for measuring loads and motions with a fixed carriage speed is short.

As explained in 2.3.2, due to experimental setup limitations, the model pitch inertia is proportionally far too high. This is believed to be the cause of very large motions observed in some of the runs. As this inertia is independent of the model displacement (due to the counterweight compensation), its ratio with the hydrodynamic added inertia and damping has an unusual value. Similarly, the inertial loads for the heave motion are highly influenced by the heave system. The setup was designed for heavier models for which the effect of the heave column and counterweight is negligible. This is a drawback of the setup and is probably the cause for the impossibility of testing the 7% steepness waves in 2DOF. However, this does not prevent to compare the measurements with simulations, as done in the next section.

4. NUMERICAL MODELING AND COMPARISON

4.1. Approach

In this part, the DVPP presented in Kerdraon *et al.* (2019, 2020) is used to simulate the tank tests and compare the results. The DVPP is based on a system-based weakly non-linear approach: the loads are computed by superposition of several components: hydrostatic, flat water hydrodynamic loads, radiation, diffraction and Froude-Krylov loads. Hydrostatic and Froude-Krylov forces are calculated by pressure integration over the instantaneous wetted surface while radiation and diffraction are based on linear models with corrections for speed and immersed geometry changes. The flat water hydrodynamic loads are computed from a response surface built from captive towing tests with the model attitude, sinkage and speed as parameters. Simulations are run with 3rd order Stokes waves.

Unlike most of the models tested on a similar setup, the implicated mass ratios do not allow to neglect the effect of the heave column or of the counterweight. However, while the model is free to both heave and pitch, these two elements can only slide vertically. To represent correctly the inertial effects at stake in the setup, a multibody approach was thus adopted. The system is made up of three bodies: the carriage, which translates horizontally at a prescribed speed, the heave system, free to translate vertically with respect to the carriage, and the model, which can pitch with respect to the heave system.

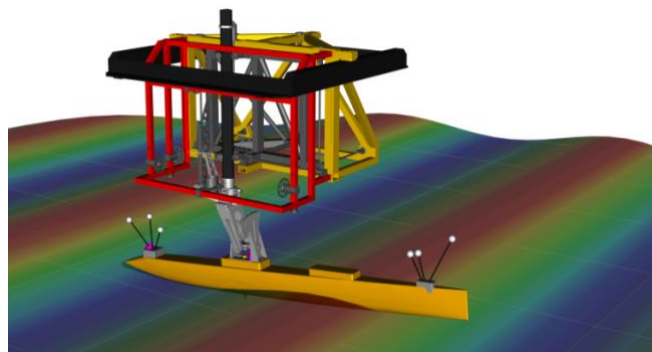
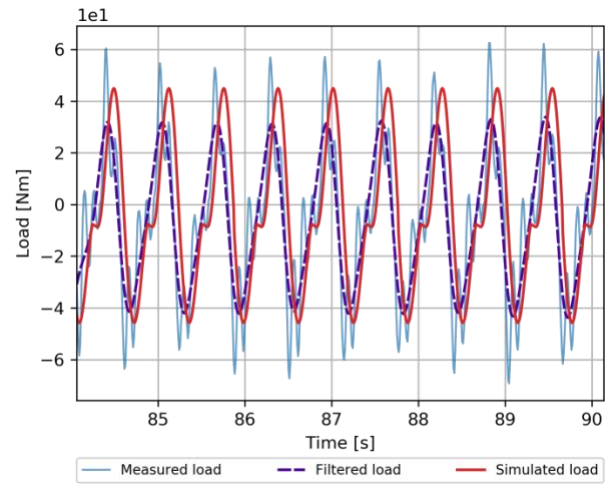
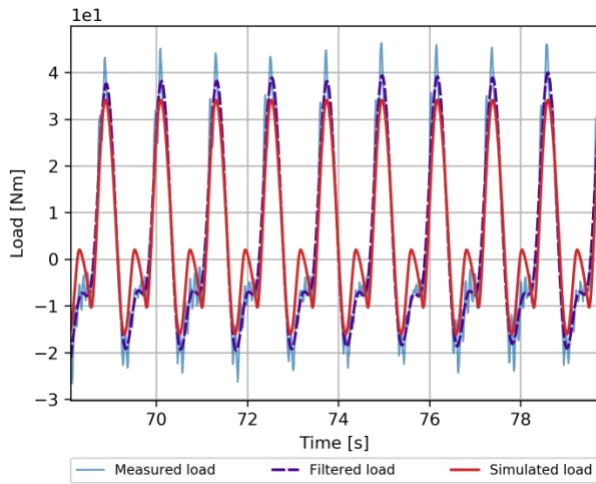
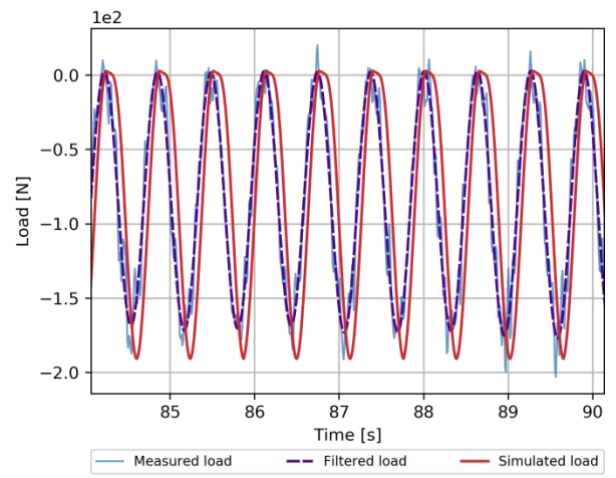
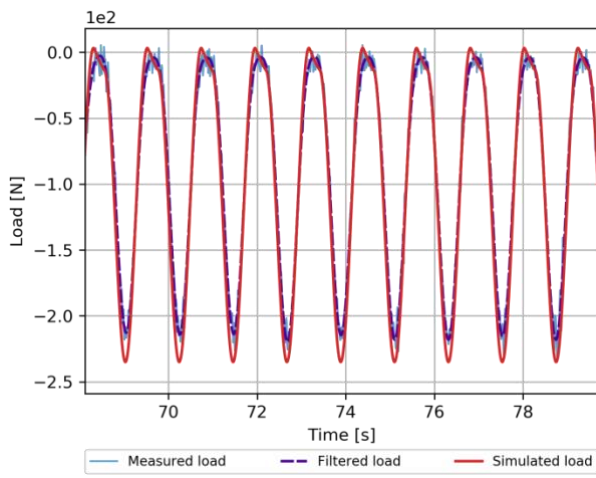
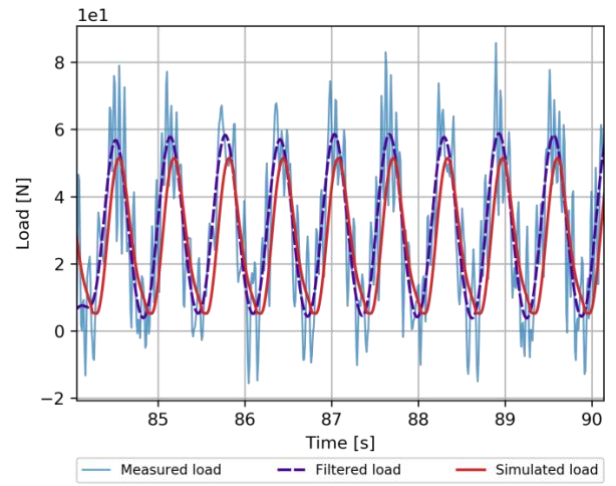
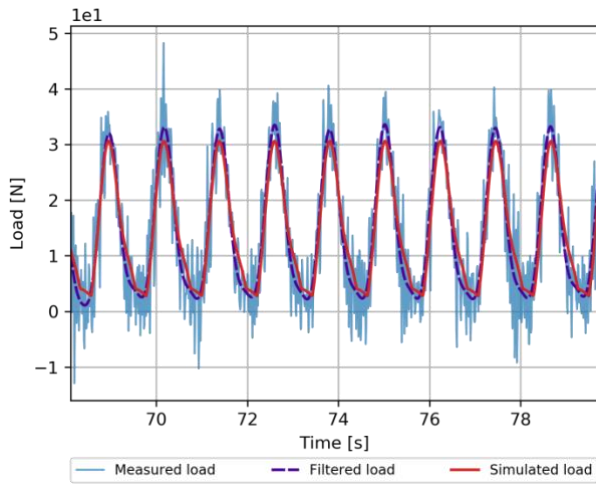


Figure 10. Tank tests numerical simulation with the DVPP.

To simplify the problem, the sheave system is neglected and the counterweight is assimilated to a mass with upwards gravity. Solid friction in the setup is neglected. Resulting simulation is shown in Figure 10.



a) $F_n = 0.81$, $\beta = 2^\circ$, $\lambda = 3.9L_{PP}$ and $S = 1.7\%$.

b) $F_n = 1.21$, $\beta = 0^\circ$, $\lambda = 2.3L_{PP}$ and $S = 3.5\%$.

Figure 11. Comparison with the DVPP for captive tests (top: surge force, middle: heave force, bottom: pitch moment).

4.2. Captive tests

In this section, heave and pitch are restrained and the measured and calculated loads are compared. As some of the measurements exhibit strong non-linearities, it is of great interest to compare the time series rather than only response amplitude operators. Simulated and measured signals are synchronized with respect to the phase of the waves. The accuracy of the excitation phase determination is thus critical to properly synchronize the signals. This is done through a least square regression which yields a maximal standard deviation of 0.015 rad for the phase. Only sequences with stabilized carriage velocity are plotted. Examples of comparison are shown in Figure 11. Correlation is good, the main features of the response are correctly retrieved and the amplitude and phase are consistent.

Out-of-plane loads (sway force F_y , heeling and yawing moments M_x and M_z) are mainly underestimated in the case with non-zero leeway. Setup deflection is believed to be a major cause of these differences. The motion tracking system measured variations of yaw up to 1.5 degrees in the most severe conditions, leading to variations of the effective leeway angle and therefore increasing the amplitude of the loads oscillations.

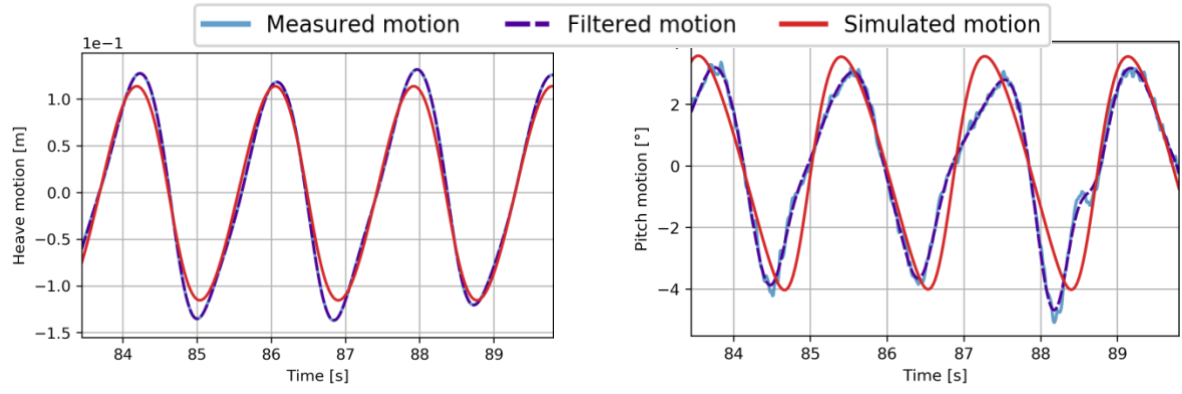
4.3. Semi-captive tests

Heave and pitch are now freed, and the measured and simulated responses are compared. As for the captive tests, motion signals are synchronized so that the excitation signals are in phase. Example results are plotted in Figure 12.

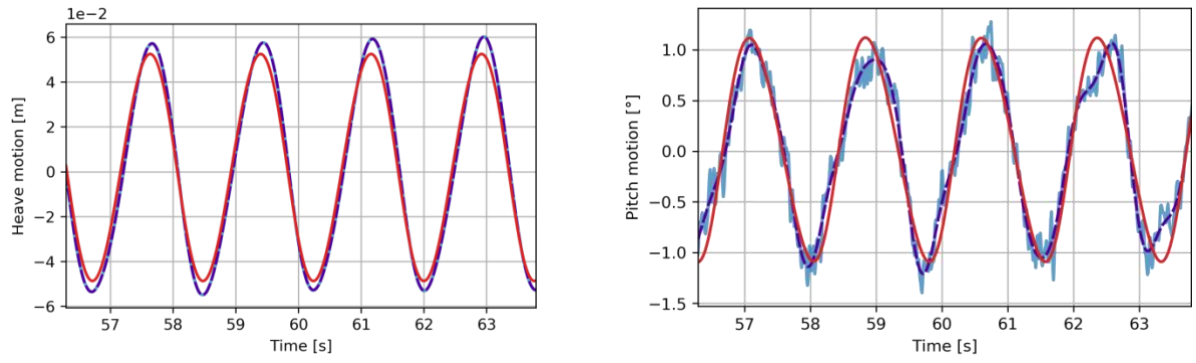
Heave motion presents a good correlation. Phases and amplitudes are consistent with the experimental results. The last presented case, which is one of the most severe conditions ($F_n = 1.2$ and wave steepness of 3.5%) suffers from the low frequency oscillations of the experimental data. However, the amplitude and phase of the heave component at the encounter frequency are rather correct.

As for the pitch motion, the correlation is not as good. Phases and amplitudes are globally consistent, but numerical responses lack specific features observed on the experimental signals. One can notice that those features are not necessarily repeated in all oscillations of the experimental data. As far as the fourth presented case, is concerned, the amplitude of the simulated pitch motion is about half of the experimental value.

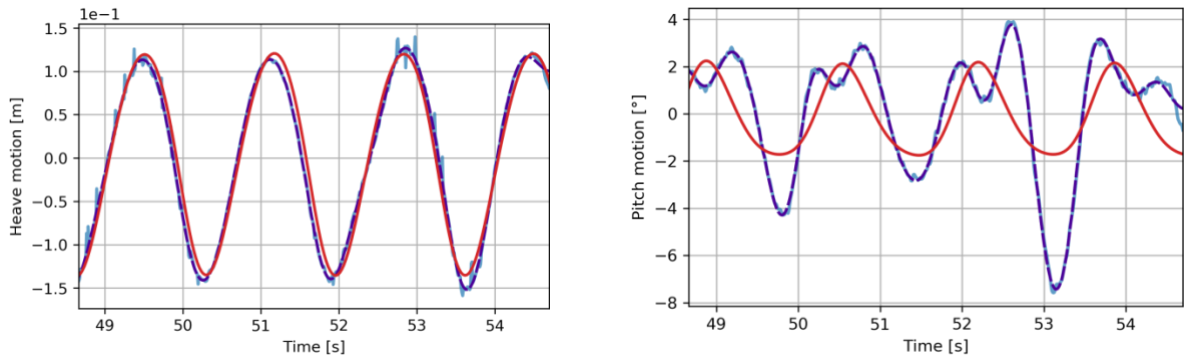
An example of surge force comparison is provided in Figure 13. The quality of the correlation between simulated and measured loads is strongly dependent on the correlation of heave and pitch responses. In the plotted results, the pitch peak (Figure 12d) is thus retrieved in the measured surge force. Overall, consistency is rather correct. It is interesting to note the evolution of the mean resistance: for this case, the flat water value is 24.2 N, while it reaches 30.4 N in captive mode and 29.1 N in semi-captive mode. Similar tendencies are observed on all points.



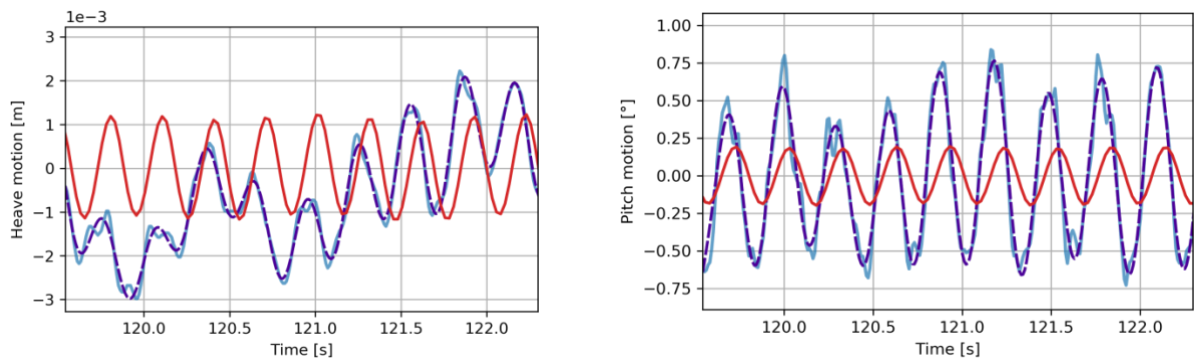
a) $F_n = 0.36$, $\beta = 2^\circ$, $\lambda = 4.6L_{PP}$ and $S = 1.7\%$.



b) $F_n = 0.81$, $\beta = 2^\circ$, $\lambda = 7.1L_{PP}$ and $S = 0.5\%$.



c) $F_n = 1.21$, $\beta = 0^\circ$, $\lambda = 9.2L_{PP}$ and $S = 0.9\%$.



d) $F_n = 1.21$, $\beta = 2^\circ$, $\lambda = 0.9L_{PP}$ and $S = 3.7\%$.

Figure 12. Comparison with the DVPP for semi-captive tests.

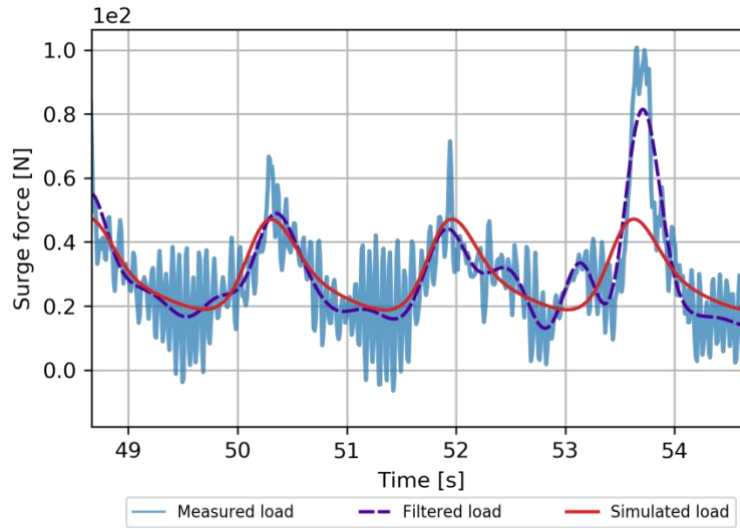


Figure 13. Surge force comparison with the DVPP in semi-captive conditions, $F_n = 1.21$, $\beta = 0^\circ$, $\lambda = 9.2L_{pp}$ and $S = 0.9\%$.

4.4. Discussion

Flat water loads were measured using the same setup and tank as the experiments in waves. They are thus subjected to similar phenomena, such as windage and shallow water effects. The loads are not corrected for these effects before building the flat water hydrodynamic loads response surface. The response surface, used in the simulations, therefore indirectly accounts for these effects. Given the important cross-section of the setup, and especially the heave and pitch system, windage has a non-negligible impact on the measured loads, especially at the highest speeds. Runs with the model in air were performed to assess them (the total cross section variation due to the model immersion is neglected). At $F_n = 1.21$, the windage drag reaches up to 4.6 N, which represents 25% of the 18.2 N of the drag force measured at that speed in the water.

As discussed previously, some of the studied speeds are too close or even beyond the critical wave velocity. This implies that finite depth effects occur at those speeds (see DeBord et al., 1990). Although we were not able to quantify the impact of this phenomenon on the loads, it is also accounted for in the flat water loads.

There is no absolute pattern that allows to discriminate parameters that would be acceptable or non-acceptable in terms of simulation accuracy. Heave motion is rather more accurately described than the pitch response. The most probable cause is that the response surface for flat water hydrodynamic loads was not built on a sufficient range of pitch values (input range is $-3/+3^\circ$, while the amplitude is beyond 6° in some cases). Thus the pitching moment variations are not described with sufficient accuracy for the largest amplitudes. Expanding the range of the input data to the response surface would probably improve the results quality and should be tested.

Solid friction in the heave and pitch system was not accounted for in the model. The measurements of vertical force and pitching moment provide an order of magnitude of the frictional effects in the setup. Their maximum variations are respectively of 3 N and 7 Nm. Considering the masses and inertia at stake in the setup, friction can indeed be neglected, which is consistent with the absence of clear overestimation of the motion by the simulator.

5. CONCLUSIONS

This paper has presented the design and methodology of an experimental campaign aiming at validating the hull model of a DVPP. A wide range of speeds and wave conditions were investigated. Loads, excitations and motions were measured with carefully calibrated sensors. Both linear and nonlinear model behaviors were observed depending on the wave conditions and model speeds, generating a large number of validation cases for the DVPP.

The main improvement point resides in the inertial effects that were too important with respect to the model displacement, due to the chosen position of the center of buoyancy and to the heave and pitch system weights.

Comparison with DVPP simulations both in fully restrained conditions and in 2DOF were carried out, showing encouraging results. The heave response is particularly well described. Discrepancies in the out-of-plane loads need further investigations to identify whether they originate from experimental issues, and particularly yaw tuning uncertainties and setup deflection, or from numerical models deficiencies.

The chosen model seems nevertheless relevant, even for simulation of the yacht behavior in the severe conditions that are high speeds and rough sea states. It would be of interest to broaden the scope of measurements with even steeper waves to get closer to the models limits as well as to improve the flat water hydrodynamic loads response surface by larger pitch angle values.

Even though high-performance yacht design is well underway towards making boats fly offshore, accuracy of hull load computation is critical to properly simulate hybrid mode sailing, as well as the touchdowns and takeoffs that are likely to happen in rough seas. Block per block validation of a system-based DVPP allows to give confidence in the quality of the results, a process that will be pursued.

Further tests were carried out in a second phase of the experimental campaign with a Stewart platform (hexapod) to study the loads in forced motions (oscillations as well as specific transient phases such as water entry). They will allow to validate other aspects of the DVPP models.

6. ACKNOWLEDGMENT

This work was supported by VPLP Design and the ANRT (French National Association for Research and Technology).

A special thanks to the LHEEA ocean tank staff for the help they provided throughout the preparation and realization of this experimental campaign.

7. REFERENCES

Allan, J. F., Doust, D. J. and Ware, B. E. (1957) Yacht testing. In *Trans. RINA*, 99.

Angelou, M. and Spyrou, K. (2017) A new Mathematical Model for investigating the Course Stability and Maneuvering motions of Sailing Yachts. *Journal of Sailing Technology*, 2(1), 1-42, The Society of Naval Architects and Marine Engineers.

Binns, J. R., Hochkirch, K., De Bord, F. and Burns, I. A. (2008) The development and use of sailing simulation for IACC starting maneuver training. 3rd High Performance Yacht Design Conference, Auckland, New-Zealand.

Clark, N. A. (2104) Validation of a sailing simulator using full scale experimental data. Master's thesis, University of Tasmania, Launceston, Australia.

Day, A.H., Cameron, P. and Dai, S. (2019) Hydrodynamic Testing of a High Performance Skiff at Model and Full Scale. *Journal of Sailing Technology*, 4(1), 17-44, The Society of Naval Architects and Marine Engineers.

Day, S., Letizia, L. and Stuart, A. (2002) VPP vs PPP: challenges in the time-domain prediction of sailing yacht performance. High Performance Yacht Design Conference, Auckland, New-Zealand.

DeBord, F. W. and Teeters, J. (1990) Accuracy, test planning and quality control in sailing yacht performance model testing. New England Sailing Yacht Symposium, New London, USA.

Gauvain, E. (2019) The un-restrained sailing yacht model tests – a new approach and technology appropriate to modern sailing yacht seakeeping. The 23rd Chesapeake Sailing Yacht Symposium, Annapolis, MD, USA.

Hansen, H., Hochkirch, K., Burns, I. and Ferguson, S. (2019) Maneuver Simulation and Optimization for AC50 Class. *Journal of Sailing Technology*, 4(1), 142-160, The Society of Naval Architects and Marine Engineers.

Horel, B. and Durand, M. (2019) Application of System-based Modellins and Simplified-FSI to a Foiling Open 60 Monohull. *Journal of Sailing Technology*, 4(1), 114-141, The Society of Naval Architects and Marine Engineers.

International Towing Tank Conference (2014) Guide to the expression of uncertainty in experimental hydrodynamics. ITTC - Recommended Procedures and Guidelines, 7.5-02-01-01.

International Towing Tank Conference (2017a) Seakeeping experiments. ITTC - Recommended Procedures and Guidelines, 7.5-02-07-02.1.

International Towing Tank Conference (2017b) Ship models. ITTC - Recommended Procedures and Guidelines, 7.5-01-01-01.

International Towing Tank Conference (2017c) Validation of maneuvering simulation models. ITTC – Recommended Procedures and Guidelines, 7.5-02-06-03.

International Towing Tank Conference (2017d) Verification and validation of linear and weakly nonlinear seakeeping computer codes. ITTC - Recommended Procedures and Guidelines, 7.5-02-07-02.5.

Kerdraon, P., Horel, B., Bot, P., Letourneur, A. and Le Touzé, D. (2019) 6DOF behavior of an offshore racing trimaran in an unsteady environment. The 23rd Chesapeake Sailing Yacht Symposium, Annapolis, MD, USA.

Kerdraon, P., Horel, B., Bot, P., Letourneur, A. and Le Touzé, D. (2020) Development of a 6-DOF Dynamic Velocity Prediction Program for offshore racing yachts. *Ocean Engineering*, 212.

Masuyama, Y. and Fukasawa, T. (2011) Tacking Simulation of Sailing Yachts with new Model of Aerodynamic Force Variation during Tacking Maneuver. *Journal of Sailboat Technology*, 2(1), 1-34, The Society of Naval Architects and Marine Engineers.

Masuyama, Y., Nakamura, I., Tatano, H. and Takagi, K. (1993) Dynamic performance of sailing cruiser by full-scale sea tests. The 11th Chesapeake Sailing Yacht Symposium, Annapolis, MD, USA.

Murdey, D. C., Molyneux, W. O. and Killing, S. (1987) Techniques for testing sailing yacht. Advances in Yacht Testing Technique, 18th International Towing Tank Conference, Kobe, Japan.